Journal of Solid State Chemistry 184 (2011) 2719–2723

Contents lists available at ScienceDirect

Journal of Solid State Chemistry

journal homepage: www.elsevier.com/locate/jssc

Synthesis and microstructural TEM investigation of $CaCu_3Ru_4O_{12}$ ceramic and thin film

Virginie Brizé [a,b,1], Cécile Autret-Lambert [a,*], Jérôme Wolfman [a], Monique Gervais [a], François Gervais [a]

[a] Université François Rabelais, LEMA, UMR 6157 CNRS-CEA, Parc de Grandmont, 37200 Tours, France
[b] STMicroelectronics, 16 rue P&M Curie, 37001 Tours, France

ARTICLE INFO

Article history:
Received 8 April 2011
Received in revised form
18 July 2011
Accepted 25 July 2011
Available online 2 August 2011

Keywords:
High density capacitors
High K material
Conductive oxide
Perovskite

ABSTRACT

$CaCu_3Ru_4O_{12}$ (CCRO) is a conductive oxide having the same structure as $CaCu_3Ti_4O_{12}$ (CCTO) and close lattice parameters. The later compound is strongly considered for high density parallel plates capacitors application due to its so-called colossal dielectric constant. The need for an electrode inducing CCTO epitaxial growth with a clean and sharp interface is therefore necessary, and CCRO is a good potential candidate. In this paper, the synthesis of monophasic CCRO ceramic is reported, as well as pulsed laser deposition of CCRO thin film onto (001) $NdCaAlO_4$ substrate. Structural and physical properties of bulk CCRO were studied by transmission electron microscopy and electron spin resonance. CCRO films and ceramic exhibited a metallic behavior down to low temperature. CCRO films were (001) oriented and promoted a CCTO film growth with the same orientation.

1. Introduction

Oxide perovskites (ABO_3) are the subject of much attention in the scientific community due to their most diverse types of physical properties [1]. The B cation determines the transport and magnetic properties, e.g. magnetoresistance (Mn) [2], superconductivity (Cu) [3] or ferroelectricity (Ti) [4], while the cations on the A-site (Ln: a trivalent lanthanide and AE a divalent alkaline-earth) change the doping level or bandwidth. The Ti compounds, e.g. (Ba, Sr)TiO_3 or $SrTiO_3$, have been widely studied for their high or even colossal permittivity ε allowing the fabrication of decoupling capacitors with enhanced capacitance per area for nomad electronics devices. One way to miniaturize capacitors at constant capacitance level is to increase the dielectric permittivity (ε) of an insulating material, as can be seen in the capacitance formula for parallel plate capacitors: $C=(\varepsilon S)/e$ (where S is the conducting plates area and e their separating distance). The highest dielectric constants are observed in ferroelectric or relaxor material. However, the dielectric constant of materials like (Ba, Sr)TiO_3 and $SrTiO_3$ strongly depends on the temperature and are maximized in the vicinity of the ferroelectric–paraelectric phase transition. For many applications, this strong temperature dependence is problematic ([5] and references therein, [6]).

Thus, materials exhibiting a high dielectric constant with low sensitivity to temperature variation are of technological importance and are highly needed. Recently, the discovery of colossal permittivity $CaCu_3Ti_4O_{12}$ (CCTO) has generated a great interest [7]. Indeed, CCTO exhibits a colossal dielectric constant ε in excess of 10^4 which remains almost constant between 100 K and 600 K in the 10^2–10^5 Hz frequency range. This was observed in single crystal [8,9], ceramic [10,11] or thin film form [12,13].

The general formula for this compound is $AC_3B_4O_{12}$. Its structure derives from the parent perovskite structure ABO_3, with three fourths of the A-site cations being substituted by Jahn–Teller active ions (Cu^{2+}). Ca (A-site) and Cu (C-site) ions are ordered and a collective rotation of BO_6 octahedra around the crystallographic [1 1 1] direction is observed. The corresponding unit cell doubles in all the three directions ($V=2a_p\cdot 2a_p\cdot 2a_p$) with respect to the cubic perovskite cell ($a_p\approx 3.8$ Å). The crystal structure of these compounds is cubic with *Im*-3 symmetry [14,15]. A large variety of cations can occupy the A and B site, whereas the C site is usually occupied by Cu^{2+} or Mn^{3+} ions [16–18]. As in the case of perovskites, the nature of the B cation changes the physical properties of the material. Materials investigated in this work are $CaCu_3Ti_4O_{12}$ (CCTO) and $CaCu_3Ru_4O_{12}$ (CCRO). The Ti compound is a semi-conductor with a high dielectric permittivity, whereas the Ru one is metallic [19]. Both materials are of potential interest to achieve thin film capacitors with CCRO as the bottom electrode and CCTO as the dielectric material. The shared structure and close lattice parameters of these two materials should lead to a decrease of the strains at the electrode/CCTO interfaces.

* Corresponding author. Fax: +33 2 47 36 71 21.
E-mail address: cecile.autret-lambert@univ-tours.fr (C. Autret-Lambert).
[1] Present address: CEA—INES, 17 rue des Martyrs, 38054 Grenoble, Cedex 9, France.

0022-4596/$ - see front matter © 2011 Elsevier Inc. All rights reserved.
doi:10.1016/j.jssc.2011.07.041

In this paper, the synthesis of polycrystalline CCRO powder and ceramic, as well as textured thin films is detailed. Structural and physical properties of CCRO in the form of both ceramic and thin films deposited on (0 0 1) $NdCaAlO_4$ (NCAO) single crystal are compared. The structural investigation of conducting $CaCu_3Ru_4O_{12}$ thin films is presented. Finally some structural results on CCTO/CCRO/$NdCaALO_4$ stack are reported.

2. Results and discussion

2.1. CCRO powder synthesis

An optimal procedure was used to prepare $CaCu_3Ru_4O_{12}$ as close to stoichiometry as possible with solid state reaction between oxides precursors: CuO_2 (Chempur 99.9%), $CaCO_3$ (Chempur 99.9%) and RuO_2 (Aldrich 99.99%). The precursors were dried in air at 400 °C for 24 h. In order to obtain the stoichiometric composition, ruthenium was introduced using a defect of 10% compared with the nominal composition. The reagents were mixed in an agate mortar then ground by ball-milling in isopropanol for one night to obtain a fine powder. The powder was cold pressed into pellets and heated at 850 °C for 10 h. The composition of resulting pellet was checked by X-ray powder diffraction which was carried out using a Bruker D8 X-ray diffractometer using Cu $K\alpha$,β radiation. At this stage, the obtained compound was not single phase. On the X-ray powder diffraction pattern (Fig. 1a), in addition to the CCRO phase indicated by arrows, three additional phases are observed: CuO (noted by a star), RuO_2 (circle) and $CaRuO_3$ (square). Thus, the pellets were again ground in an agate mortar and then mixed in isopropanol before being pressed. This new pellet was annealed at higher temperature, i.e. 900 °C during 10 h. This grinding, pressing and annealing sequence was repeated several times. X-ray diffraction patterns recorded after each annealing step at 900 °C are shown Fig. 1 b, c and d. During the subsequent annealing, the impurities gradually disappear to finally obtain a CCRO compound without any indication of impurity.

2.2. Characterization of the CCRO powder

The Rietveld method using the Fullprof program [20] was employed to refine the structural and profile parameters. A pseudo-Voigt function was chosen for the line shape of the diffraction peaks.

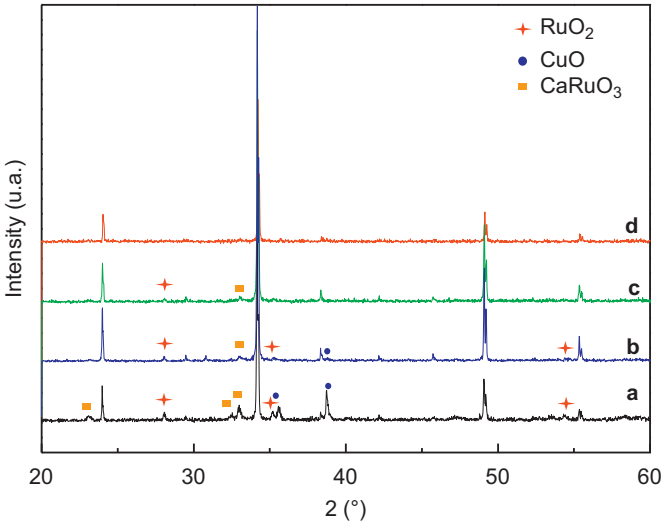

Fig. 1. X-ray diffraction of $CaCu_3Ru_4O_{12}$ powders with different annealing (a), 850 °C (b, c, d), 900 °C–10 h.

Lattice parameters, positional coordinates, isotropic thermal and occupancy factors were refined. The structural refinements of room temperature X-ray diffraction data were performed in the space group *Im*-3, which is characterized by cell parameters that are doubled compared to the unit cell of the ideal cubic perovskite structure [18,19]. A cell parameter $a=7.4177(5)$ Å was found, with reliability factors $R_{Bragg}=7.57\%$ and χ^2 close to 2.98. The atoms are located at the following Wyckoff positions: Ca in 2*a* (0 0 0), Cu in 6*b* (0 1/2 1/2), Ru in 8*c* (1/4 1/4 1/4), and O in 24*g* ($x=0.3152(1)$, $y=0.1967(2)$, 0) sites. The deviation from the ideal values of x and y equal to 0.25 causes the rotation of the octahedral around [1 1 1] axis.

The sample was prepared for transmission electron microscopy (TEM) from pellet by crushing the bars in alcohol. The small crystallites in suspension were then deposited on a holey carbon film, supported by a nickel grid. The specimens were examined at room temperature using a JEOL 2100 FEG microscope (200 kV and point resolution of 1.8 Å) equipped with a tilting and rotating goniometer. Calculated images were obtained using JEMS program [21]. The EDS analyses confirmed a good homogeneity and a cationic composition close to the nominal composition, in the limit of the experimental error, and taking into account a lack of 10% RuO_2 compared to the formula $CaCu_3Ru_4O_{12}$ as Labeau et al. had suggested [19].

Selected area electron diffraction (SAED) has been used to reconstruct the reciprocal space, confirming the above unit cell $a \approx 2a_p$ (a_p is the parameter of a cubic perovskite subcell). Reflection conditions are compatible with space group *Im*-3 (No 204) which are: *h k l*: $h+k+l=2n$, *h k* 0: $h+k=2n$, *h* 0 0: $h=2n$, 0 *k* 0: $k=2n$, 0 0 *l*: $l=2n$. Both characteristic diffraction patterns with the zone axis [0 0 1] and [-1 1 0] are shown Fig. 2a and b. No extra reflections can be observed on the patterns.

The high resolution electron microscopy (HREM) performed on a few crystallites confirms the high quality of its crystallization. The comparison of the experimental HREM images with those calculated from positional parameters deduced from XRD refinements shows a good fit. The HREM image presented in Fig. 3a shows a large view of the crystal with a uniform background contrast. No defects can be seen along the stack axis. The corresponding [0 0 1] HREM image (Fig. 3b) exhibits a contrast which consists in a very regular array of bright dots depicting the high electronic density zones. In the enlarged HREM image the light dots are assimilated to ruthenium positions (inset Fig. 3b). The bright spots spacing is about 5.2 Å along ⟨1 1 0⟩. Such images attest to a statistical distribution of the cations.

Electron spin resonance (ESR) measurements have been performed on both CCTO and CCRO samples with a Bruker EMX 10/2.7 in the X-band (9.5 GHz). The spectrum from the Cu^{2+} ($3d^9$) paramagnetic cation (spin 1/2) of pure CCTO sample consists of a single signal centered at $g \approx 2.14$ with a Lorentzian line-shape (Fig. 4). The linewidth of ESR line is confirmed to be unexpectedly narrow, about 34 G. The origin of the narrow signal has been discussed in a previous paper [22]. An exchange narrowing related to thermally activated phenomenon was proposed to explain this signal. In the [1 1 1] direction, there is a stack of planes containing 3 equivalent Cu between which lies Ti cation (inset Fig. 4). The level of conductivity suggests a hopping motion of the copper d electrons from Cu site to Cu site on these planes [22]. Copper *d* conducting electrons randomize the dipolar interactions of their spins and might induce line narrowing. CCTO bulk as a whole remains semi-conductor. Other possibilities were proposed in the literature, for example the oxygen stoichiometry [23,24]. Pires et al. [23] found a correlation between line broadening and the conditions that create oxygen vacancies. The CCRO compound was also studied by ESR (Fig. 4). Many compounds containing Ru^{4+} and Ru^{5+} ions in octahedral coordination have

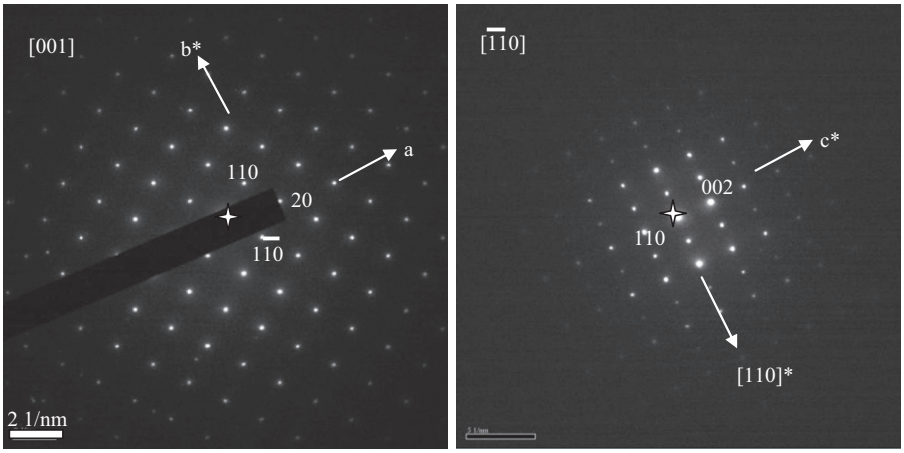

Fig. 2. [0 0 1] and [-1 1 0] electron diffraction patterns of the $CaCu_3Ru_4O_{12}$.

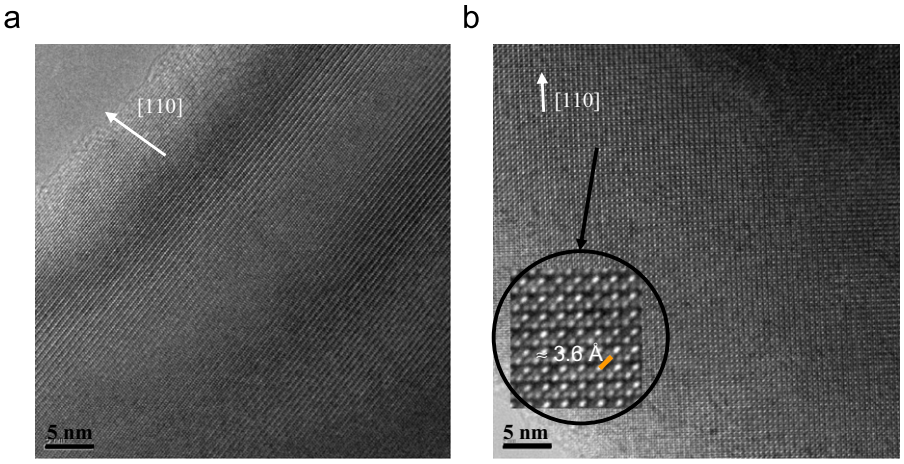

Fig. 3. (a) [1 1 0] lattice image corresponding to the ED pattern given in Fig. 2 and (b) [1 1 0] HREM image recorded for $CaCu_3Ru_4O_{12}$. A very regular contrast is observed, which attests to the statistical distribution of the cations, anions and vacancies over their respective sites. In inset, the bright dots correspond to the Ru cation.

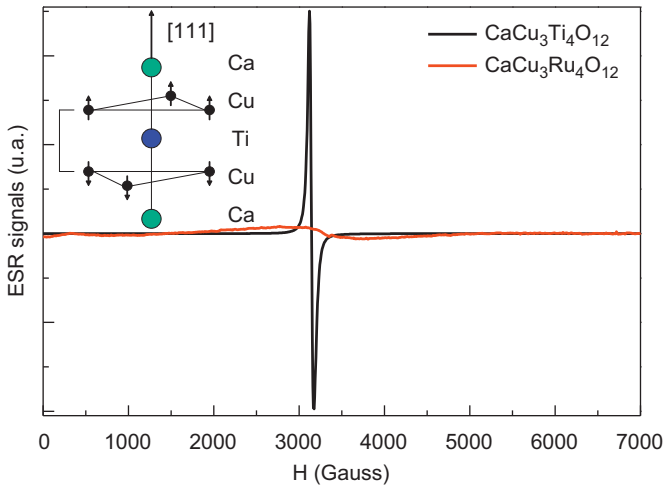

Fig. 4. ESR spectra of $CaCu_3Ti_4O_{12}$ (a) and $CaCu_3Ru_4O_{12}$ (b) samples at room temperature from 0 to 7000 G. In inset, schematic arrangement of cations in $CaCu_3Ti_4O_{12}$ along the [1 1 1] direction. Arrows indicate the AFM order at low temperature.

been studied by ESR at a frequency of 35 GHz. The results showed that Ru is ESR silent due to the large crystal-field [25]. Thus only the square planar Cu^{2+} coordination might give a signal. But, a surprising feature encountered in this oxide is the absence of an electron paramagnetic resonance signal despite the presence of Cu^{2+} species which is one of the easiest to observe at least in insulators, like CCTO. This fact was already observed in the superconductor materials such as $YBa_2Cu_3O_7$ containing CuO_2 planes [26,27]. So far, no convincing mechanism has been proposed to explain the ESR silence with a conventional ESR spectrometer at any temperature (from 70 K to 1150 K) [26]. Thus for CCRO, either ESR signal is absent, or the linewidth is too broad to be observed with conventional ESR spectrometers at 9 GHz.

Ref. [28] suggests that CCRO is a *d*-electron heavy fermion system whose behavior comes from the Kondo mechanism. In this scenario, Cu 3*d* electrons are localized while Ru 4*d*, electrons contribute to the conduction [28]. As described for CCTO, the thermal activation of the Cu 3*d* electron motions would tend to narrow the line. The fact that the electrons of Cu 3*d* for CCRO are localized results in broadening of the signal. This is in agreement with the hypothesis of exchange narrowing. Moreover, CCRO shows a metallic Pauli paramagnetism, 4*d* conduction electrons of Ru can move almost freely, being only very weakly bound to atoms of metal. This motion of electron could be observed by ESR. However CCRO has a metallic character and ESR anomalies accompanying such a character are the disappearance or a large broadening of the signal [29]. The strong interactions between the localized and itinerant electrons lead to a short relaxation time enlarging the signal. Finally, we could suppose that a signal exists but it is too large to be seen with the conventional instrument.

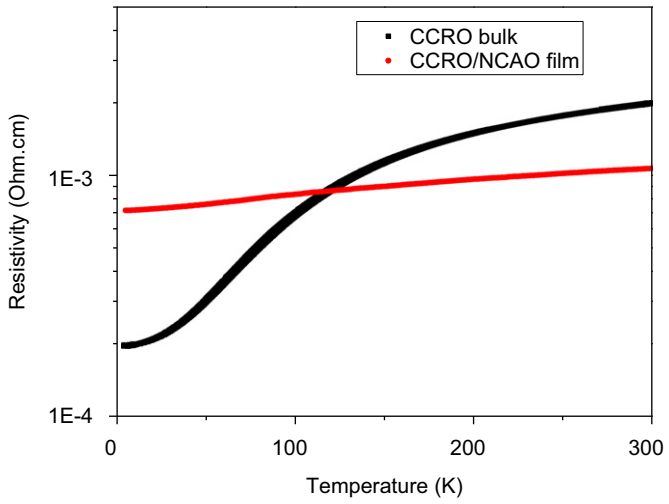

Fig. 5. Temperature dependence of the electrical resistivity for bulk and thin film samples of $CaCu_3Ru_4O_{12}$.

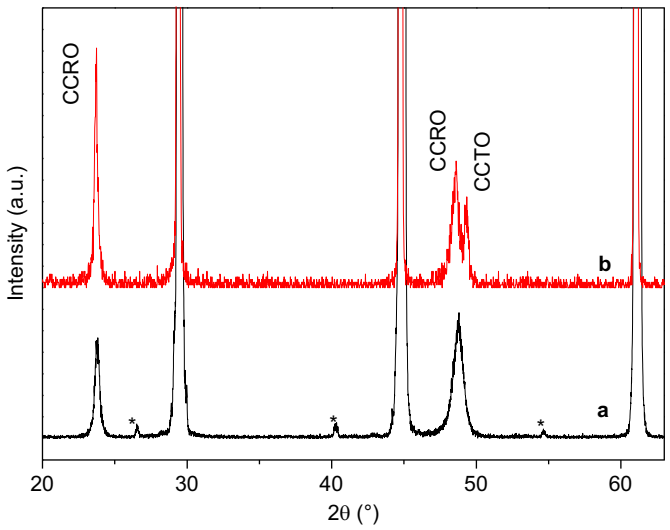

Fig. 6. X-ray diffraction pattern at room temperature (a) $CaCu_3Ru_4O_{12}$ thin film on $NdCaAlO_4$, asterisks represent the K_β of the substrate and (b) $CaCu_3Ti_4O_{12}$/$CaCu_3Ru_4O_{12}$/$NdCaAlO_4$ stack.

However, the interpretation of this phenomenon requires further experiments.

The resistances versus temperature measurements were performed with a Physical Property Measurements System (PPMS) using a standard four probe method. Electrical resistivity of CCRO target is shown in Fig. 5. It can be observed that the compound exhibits a metallic behavior with $d\rho/dT > 0$. The value of the resistivity at 300 K is close to 2 mΩ cm in agreement with the literature [19].

The conductive nature of this material makes it a potential electrode for CCTO based thin film capacitor. In order to achieve an epitaxial growth with minimum stress, we examined the list of commercially available single crystal substrates having a close lattice parameter match with both CCRO and CCTO. The closest match was found to be with (0 0 1) oriented $NdCaAlO_4$ (NCAO) substrates. NCAO has a lamellar structure similar to K_2NiF_4 i.e. a succession of perovskite and rocksalt layers in the c direction. Consequently NCAO is tetragonal with $a=b=3.685$ Å and $c=12.12$ Å. For (0 0 1) oriented NCAO substrate, CCRO growth would occur on NCAO (a,b) plane whose lattice parameter has to be compared to half the CCRO and CCTO lattice parameter, i.e. $c/2 \approx 3.709$ Å and $c/2 \approx 3.691$ Å, respectively. The mismatch between (0 0 1) NCAO and CCTO (-0.1%) is thus much smaller than the one between CCTO and the most commonly used substrate for CCTO growth, i.e. $LaAlO_3$ (2.3% with a pseudo cubic cell parameter $a \approx 3.79$ Å). Synthesis of thin CCRO films onto NCAO was attempted by pulsed laser deposition (PLD).

2.3. CCRO film deposited on (0 0 1)-NCAO

Single phased CCRO powder was uniaxially pressed into a disk form at a pressure of 15 ton. The pressed disk was annealed at 900 °C for 20 h, leading to a density of 57% of the theoretical value. This low density value is due to the selected low sintering temperature in order to limit Cu volatility. The resulting pellet was used as a target to deposit thin films. The films were grown on (0 0 l) NCAO substrate by PLD with a KrF laser ($\lambda=248$ nm). The repetition rate was 20 Hz and the energy density was 3 J/cm^2. Thin films were deposited at 600 °C with a dynamic oxygen pressure $P_{O2}=0.005$ mbar. After deposition, films were cooled slowly in the chamber to room temperature under a static oxygen pressure of 500 mbar.

X-ray diffraction pattern of one CCRO thin film (Fig. 6a) shows, in addition to NCAO substrate peaks, two additional peaks at $2\theta=23.8°$ and $2\theta=48.8°$. These 2θ values correspond to (0 0 2) and (0 0 4) CCRO peak positions. No additional peak either due to another orientation or an impurity can be observed on the X-ray diagram. Small additional peak marked by asterisks corresponds to $K\beta$ peaks of the NCAO substrate. We can conclude from that that only (0 0 l) oriented CCRO phase is present.

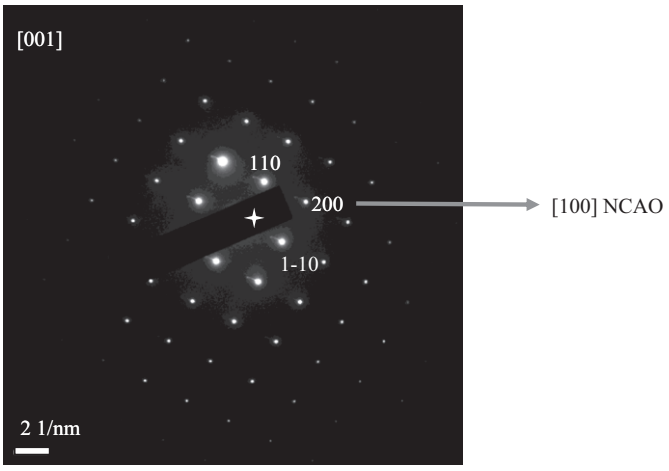

Fig. 7. [0 0 1] ED pattern of $CaCu_3Ru_4O_{12}$ on $NdCaAlO_4$.

Some crystallites were scratch off the film surface and observed in plane view geometry by TEM (same equipment as before). The electron diffraction was recorded along a direction perpendicular to the substrate plane. A single ED pattern corresponding to a [0 0 1] zone-axis is observed (Fig. 7). This implies that a and b axis of the film are aligned with a and b axis of the substrate, or in other words that CCRO growth is epitaxial. This is not surprising taking account the small lattice mismatch and the structure closeness. In the HREM image recorded along the [0 0 1] zone-axis shown in Fig. 8, a good crystalline quality is observed as shown by the nice atomic rows arrangement and the lack of defects over a large zone. Furthermore the homogeneous contrast seen across this zone indicates that little stress is present in the deposited film.

The resistivity versus temperature curve of the CCRO film is shown in Fig. 5b. The film shows a metallic behavior in the whole temperature range down to 4 K. The different resistivity temperature dependence for CCRO bulk and film probably originate from less

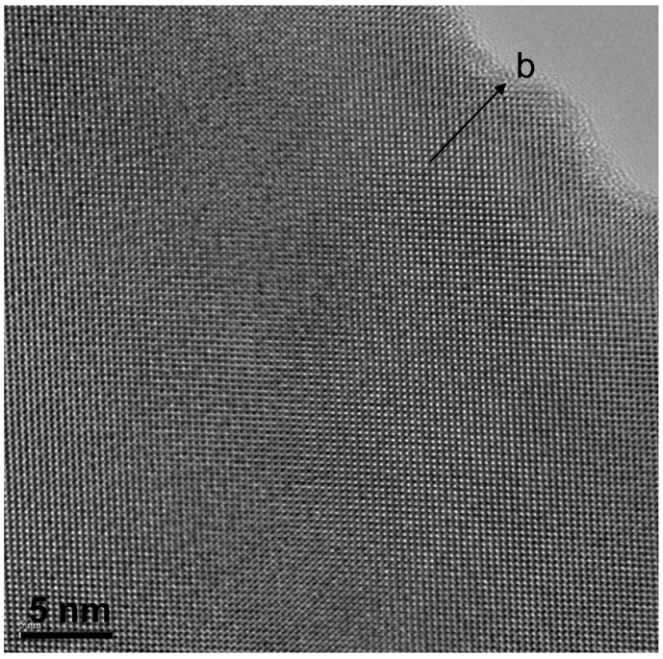

Fig. 8. [1 1 0] HREM image recorded for $CaCu_3Ru_4O_{12}$ on $NdCaAlO_4$.

perturbated grain boundaries associated to a slight epitaxial stress in the film. The room temperature resistivity (1 mΩ cm) makes CCRO film a good candidate for an electrode in an all oxide epitaxial CCTO based capacitor. So, at this stage the first deposition of CCTO on CCRO was attempted.

2.4. CCTO/CCRO/NCAO stack

The CCTO/CCRO stack was pulsed laser deposited onto NCAO substrate. The deposition conditions for CCRO were the same as those used previously (600 °C; 0.005 mbar O_2) while for CCTO, the temperature was 715 °C and the oxygen pressure 0.1 mbar. A previous investigation has shown that these conditions led to well crystallized single phased CCTO without defects. On the diffraction diagram (Fig. 6b), a peak located at $2\theta \approx 48.6^\circ$, can be associated with CCRO (0 0 4) diffraction peak. On the right side of the peak a second reflection ($2\theta \approx 49.4^\circ$) can be assigned to (0 0 4) of CCTO phase. The gap between the positions of the peaks is relevant to the slight difference between the lattice parameters of CCRO ($c/2 \approx 3.709$ Å) and CCTO ($c/2 \approx 3.691$ Å). This lattice parameters difference is probably due to the size difference between Ru^{4+} and Ti^{4+}, respectively, 0.62 and 0.60 Å. Both CCTO and CCRO are (0 0 l) oriented. We have seen in Fig. 7 that CCRO grew epitaxially onto NCAO, and we can assume that it remains the same when CCTO is grown on top of CCRO/NCAO. The in-plane lattice parameters of NCAO and CCRO were identical within the experimental resolution. This implies that CCRO is experiencing a small compressive stress onto NCAO resulting in a probable elongation of its c parameter, i.e. a shift toward lower 2θ values of the (0 0 4) peak position. Indeed the peak position $2\theta \approx 49.4^\circ$ corresponds to a parameter $c \approx 3.744$ Å, i.e. slightly higher than CCRO lattice parameter. In the case of CCTO, the compressive stress is almost non-existent; hence the increased gap between CCRO and CCTO (0 0 4) peaks.

3. Conclusion

Single-phase polycrystalline $CaCu_3Ru_4O_{12}$ powder and ceramic have been synthesized. X-ray diffraction and transmission electron microscopy studies have confirmed that CCRO and CCTO share a similar structure. CCRO was verified to be a conductive oxide, with a room temperature resistivity of 2 mΩ cm. Most noticeably, no electron spin resonance signal was detected. The absence of an ESR signal for CCRO contrasts with the narrow signal evidenced for the semi-conducting CCTO. CCRO sintered powder was used as a target to deposit thin film on NCAO single crystal. Results of X-ray diffraction, TEM and HREM are consistent with a single-phased CCRO film having a cube-on-cube epitaxy relationship with the substrate. CCRO thin film displayed a conductive behavior too, with a reduced room temperature resistivity (1 mΩ cm) compared to the sintered powder. CCRO film is thus particularly interesting as an electrode material for CCTO based thin film capacitor. CCTO/CCRO stacks have been grown onto NCAO substrate. CCTO and CCRO appeared to be single-phased and (0 0 l) oriented. A comparison of the electrical properties of CCTO based capacitors with different electrode materials is the subject of our next paper which will be submitted soon.

References

[1] L.G. Tejuca, J.L.G. Fierro, Properties and applications of perovskites-type oxides, Marcel Dekker, New-York, 1993.
[2] R. Von Helmont, J. Wecker, B. Holzapfel, L. Schultz, K. Samwer, Phys.Rev. Lett. 71 (1993) 2332.
[3] M.K. Wu, J.R. Ashburn, C.J. Torng, P.H. Hor, R.L. Meng, L. Gao, Z.J. Huang, Y.Q. Wang, C.W. Chu, Phys. Rev. Lett. 58 (1987) 908.
[4] W.J. Merz, Phys. Rev. 76 (1949) 1221.
[5] F. Iona, G. Shirane, Ferroelectric Crystals, Pergamon, New-York, 1962; M.E. Lines, A.M. Glass, Principles and Applications of Ferroelectrics and Related Materials, Clarendon, Oxford, 1977.
[6] S.A.T. Redfern, J. Phys.: Condens. Matter 8 (1996) 8267.
[7] M.A. Subramanian, D. Li, N. Duan, B.A. Reisner, A.W. Sleight, J. Solid State Chem. 151 (2000) 323.
[8] C.C. Homes, T. Vogt, S.M. Shapiro, S. Wakimoto, A.P. Ramirez, Science 293 (2001) 636.
[9] J. Li, A.W. Sleight, M.A. Subramanian, Solid State Commun. 135 (2005) 260.
[10] A.P. Ramirez, M.A. Subramanian, M. Gardel, G. Blumberg, D. Li, T. Vogt, S.M. Shapiro, Solid State Commun. 115 (2000) 217.
[11] T.B. Adams, D.C. Sinclair, A.R. West, Adv. Mater 14 (2002) 1321.
[12] W. Si, E.M. Cruz, P.D. Johnson, P.W. Barnes, P. Woodward, A.P. Ramirez, Appl. Phys. Lett. 81 (2002) 2056.
[13] A. Tselev, C.M. Brooks, S.M. Anlage, H. Zheng, L. Salamanca-Riba, R. Ramesh, M.A. Subramanian, Phys. Rev. B 70 (2004) 144101.
[14] S.G. Ebbinghaus, A. Weidenkaff, R.J. Cava, J. Solid State Chem. 167 (2002) 126.
[15] S. Krohns, J. Lu, P. Lunkenheimer, V. Brize, C. Autret-Lambert, M. Gervais, F. Gervais, F. Bouree, F. Porcher, A. Loidl, Eur. Phys. J. B 72 (2009) 173.
[16] B. Bochu, M.N. Deschizeaux, J.C. Joubert, A. Collomb, J. Chenavas, M. Marezio, J. Solid State Chem. 29 (1979) 291.
[17] B. Bochu, J.L. Buevoz, J. Chenavas, A. Collomb, J.C. Joubert, M. Marezio, Solid State Commun. 36 (1980) 133.
[18] Z. Zeng, M. Greenblatt, M.A. Subramanian, M. Croft, Phys. Rev. Lett. 82 (1999) 3164.
[19] M. Labeau, B. Bochu, J.C. Joubert, J. Chenavas Marezio, J. Solid State Chem. 33 (1980) 257.
[20] J. Rodriguez-Carjaval, Physica B 192 (1993) 55.
[21] P. Stadelmann. JEMS: Java Electron Microscopy Software, 2007. Available from: 〈http://cime.www.epfl.ch/people/stadelmann/jemswebsite/jems.html〉.
[22] V. Brizé, C. Autret-Lambert, J. Wolfman, M. Gervais, P. Simon, F. Gervais, Solid State Sci. 11 (2009) 875.
[23] M.A. Pires, C. Israel, W. Iwamoto, R.R. Urbano, O. Agüero, I. Torriani, C. Rettori, P.G. Pagliuso, L. Walmsley, Z. Le, J.L. Cohn, S.B. Oseroff, Phys. Rev. B 73 (2006) 224404.
[24] M.C. Mozzati, C.B. Azzoni, D. Capsoni, M. Bini, V. Massarotti, J. Phys. C 15 (2003) 7365.
[25] H.A. Blackstead, W.B. Yelon, M. Kornecki, M.P. Smylie, P.J. McGinn, Q. Cai, B.W. Benapfl, S.D. Knust, J. Magn. Magn. Mater. 321 (2009) 3207.
[26] P. Simon, J.M. Bassat, S.B. Oseroff, Z. Fisk, S.-W. Cheong, A. Wattiaux, S. Schultz, Phys. Rev. B 48 (1993) 4216.
[27] V. Kataev, K.-Y. Choi, M. Grüninger, U. Ammerahl, B. Büchner, A. Freimuth, A. Revcolevschi, Phys. Rev. L 86 (2001) 2882.
[28] T.T. Tran, K. Takubo, T. Mizokawa, W. Kobayashi, I. Terasaki, Phys. Rev. B 73 (2006) 193105.
[29] George Feher, A.F. Kip, Phys. Rev. 98 (1955) 337.